Kicked Rydberg atom: Response to trains of unidirectional and bidirectional impulses

B. E. Tannian, C. L. Stokely, and F. B. Dunning
Department of Physics and Astronomy and the Rice Quantum Institute, Rice University, 6100 Main Street, Houston, Texas 77005-1892

C. O. Reinhold, S. Yoshida, and J. Burgdörfer*
Physics Division, Oak Ridge National Laboratory, Oak Ridge, Tennessee 37831-6373
and Department of Physics, University of Tennessee, Knoxville, Tennessee 37996-1200
(Received 3 April 2000; published 11 September 2000)

The behavior of Rb($390p$) atoms subject to a train of up to 50 half-cycle pulses (HCPs) with duration $T_p \ll T_n$, where T_n is the classical electron orbital period, is investigated. In this limit, each HCP simply delivers an impulsive momentum transfer or ''kick'' to the electron. The response of atoms to a series of unidirectional kicks and to a series of kicks that alternate in direction is compared. For unidirectional kicks, the Rydberg atom survival probability has a pronounced maximum when the pulse repetition frequency v_p is $\sim$1.3 times the classical orbital frequency v_n. Classical simulations show this behavior provides a signature of dynamical stabilization. Evidence of dynamical stabilization and chaotic diffusion is also found in the distribution of final bound states. Very different behavior is observed for alternating kicks. The survival probability generally increases with v_p, although a small local maximum is evident when $v_p \sim v_n$. Little evidence of dynamical stabilization is observed in either the calculated dependence of the survival probability on the number of applied kicks, in the measured final bound-state distribution, or in the classical phase space of the kicked atom. Model calculations for a one-dimensional ''atom'' reveal islands of stability, but their three-dimensional counterparts are found to be unstable.

PACS number(s): 32.80.Rm, 42.50.Hz

I. INTRODUCTION

Studies of the behavior of impulsively driven, or ''kicked,'' systems in which the duration of each impulse is short compared to the period of the unperturbed system can provide valuable insights into nonlinear dynamics in Hamiltonian systems. Impulsively driven systems, which include the kicked rotor and the kicked hydrogen atom, are straightforward to model numerically because their time evolution can be reduced to a sequence of discrete maps between adjacent kicks. This allows detailed exploration of the long-term evolution of the system using both classical and quantum dynamics. Although systems subject to sinusoidal perturbations have been widely studied, for example, hydrogen Rydberg atoms in a microwave field [1], experimental realizations of kicked systems are few. Recently, however, atoms cooled in a standing light wave have provided a practical example of the one-dimensional standard map and have demonstrated the existence of Anderson localization in the translational motion of a single atom [2,3]. The kicked atom has been realized experimentally [4] by exposing very-high-n potassium Rydberg atoms to a sequence of equispaced unidirectional electric-field pulses, termed half cycle pulses (HCPs), whose duration T_p is short compared to the classical electron orbital period T_n. In the limit that $T_p \ll T_n$, a single electric-field pulse $\vec{F}_{\rm HCP}(t)$ simply delivers an impulsive momentum transfer or ''kick'' $\Delta\vec{p} = -\int_0^\infty \vec{F}_{\rm HCP}(t)dt$ to the excited electron. (Unless otherwise stated, atomic units are used throughout.)

Earlier studies of the kicked atom utilized K(np) atoms with $n \sim 388$, for which the classical orbital frequency v_n is $\sim$110 MHz and the orbital period T_n is $\sim$9 ns. The performance of the pulse generator used to generate the HCPs, however, limited measurements to scaled frequencies $v_0 \equiv v_p/v_n \lesssim 2$ and to scaled pulse widths $T_0 \equiv T_p/T_n \gtrsim 0.2$, barely in the impulsive limit ($T_p/T_n \ll 1$). Nonetheless, these measurements showed that the Rydberg atom survival probability following application of a train of HCPs can be surprisingly large. Further, the observed survival probabilities [4] depended markedly on the pulse repetition frequency, increasing with increasing frequency to a maximum at scaled frequencies v_0 of $\sim$1–2. This behavior was well reproduced by both one-dimensional (1D) and three-dimensional (3D) CTMC simulations, which showed that the phase space of the kicked atom contains sizable regular islands that lead to dynamical stabilization.

In the present work, measurements are extended to higher scaled frequencies, $v_0 \sim 4$, and to shorter HCP widths, $T_p \sim 500$ ps full width at half maximum (FWHM). The availability of shorter pulse widths ($T_p/T_n \sim 0.05$) provides better access to the (near) impulsive limit. The data at the higher scaled frequencies show that, after reaching a maximum at $v_0 \sim 1.3$, the survival probability begins to decrease. This behavior was predicted by 3D CTMC simulations and provides a signature of dynamical stabilization [4]. These calculations showed that, depending on scaled frequency, ionization is either chaotic or is characterized by a mixed phase space with various families of fully stable islands within which the atom is stable against ionization. A simplified 1D model was found whose behavior mirrors the 3D classical system. Signatures of stabilization and of chaotic diffusion were found in the calculated dependence of the survival probability on N, the number of applied kicks (HCPs), and in the measured

*Present address: Institute for Theoretical Physics, Vienna University of Technology, A1040 Vienna, Austria.

 ©2000 The American Physical Society

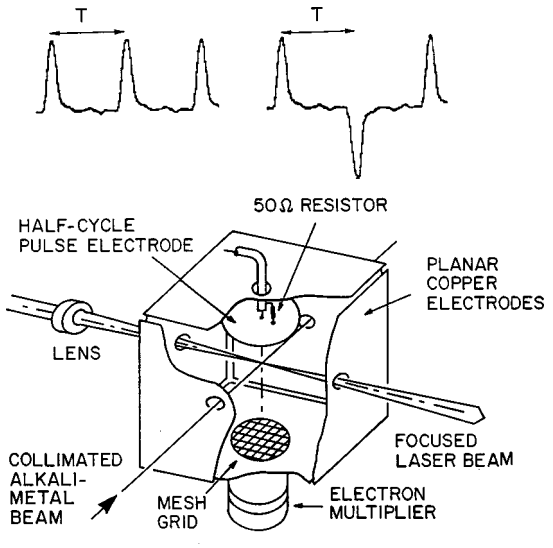

FIG. 1. Schematic diagram of the apparatus. The inset shows typical segments of the HCP trains used in this work.

n distribution of the surviving bound states.

Measurements are also extended to include trains of HCPs that alternate in sign, i.e., that provide kicks that alternate in direction. The dependence of the Rydberg atom survival probability on scaled frequency is observed to be very different from that for unidirectional kicks. In general, the survival probability simply increases with increasing scaled frequency, although a narrow local maximum is evident for scaled frequencies $v_0 \sim 1$. The data, and local maximum, are well reproduced by 3D CTMC simulations. However, these simulations show that the phase space for the system does not contain any sizable stable islands, indicating that dynamical stabilization is very unlikely. This is confirmed by calculations of the *N* dependence of the survival probability and by measurements of the final bound-state distributions. 1D simulations show that the phase space of the 1D ''atom'' contains sizeable stable islands that are associated with dynamical stabilization and the periodic ''orbit'' associated with the largest island is identified. 3D cantori and periodic orbits that correspond to the 1D islands are identified but these are found to be unstable for initial Rydberg states with very small scaled *z* components of orbital angular momentum ($L_{z0}=L_z/n \sim 0$).

II. EXPERIMENTAL METHOD

The present apparatus [4] is shown schematically in Fig. 1. Rb($390p$) atoms are created by photoexciting ground-state Rubidium atoms contained in a tightly collimated thermal-energy beam using a frequency-stabilized intracavity-doubled coherent CR 699-21 Rh6G dye laser. (Rubidium is used in the present work because the oscillator strength for excitation to high-*n* levels is significantly larger than that for potassium, resulting in increased signal levels.) Excitation occurs near the center of an interaction region bounded by three pairs of copper electrodes, each 10×10 cm. The use of large electrodes well separated from the experimental volume minimizes the effect of patch fields associated with nonuniformities in the electrode surfaces. The HCPs are generated by applying voltage pulses to a circular copper electrode 5 cm in diameter that is positioned 2.5 cm below the upper rectangular electrode. The HCP electrode is mounted on the end of a section of semirigid coaxial cable that is terminated by a 50-Ω resistor at the electrode. This arrangement minimizes the stray capacitance of the HCP electrode, allowing fast pulse rise times to be obtained. Also, the symmetry of the interaction region is reduced, limiting the excitation of resonant cavity modes. Even with all electrodes grounded, however, fields of ~ 2 mV cm^{-1} remained in the experimental volume. These were locally reduced to $\lesssim 50$ μV cm^{-1} by application of small bias potentials to the electrodes that were determined using a technique based on the Stark effect. To minimize motional electric fields, the magnetic field is reduced to $\lesssim 20$ mG by use of μ-metal shields.

Measurements are conducted in a pulsed mode. The laser output is formed into a train of pulses of ~ 4-μs duration and ~ 25-kHz repetition frequency using an acousto-optic modulator. (The probability that a Rydberg atom is formed during any laser pulse is small, $\lesssim 0.05$, and data must be accumulated following many pulses.) Excitation occurs in (near) zero electric field. Approximately 200 ns after each laser pulse, the atoms are subject to a train of HCPs that is produced using a Hewlett-Packard model 8131A pulse generator. The output pulses from the generator are ac coupled to the HCP electrode to prevent small drifts in the output baseline from introducing stray fields in the experimental volume. The pulse shapes and amplitudes are measured directly at the HCP electrode using a fast probe and sampling oscilloscope. To maintain a constant pulse shape, the amplitude of the pulses is varied using broadband attenuators connected in series with the pulse generator. Segments of the pulse trains used in the present work are included in Fig. 1. Each HCP has a duration of ~ 500 ps FWHM with rise and fall times of ~ 200 ps.

One problem when using very short HCPs is that of relating the actual time-dependent electric field experienced by the excited electron, and the impulse it receives, to the voltage pulse applied to the HCP electrode. For sufficiently long pulses, the electric field can be determined to good accuracy by solving Laplace's equation with the appropriate boundary conditions. In the present case, however, the pulse duration is only twice the transit time of an electromagnetic pulse across the interaction region. Calculation of the electric field therefore requires solution of the full Maxwell's equations. Rather than attempt this, an alternate approach was adopted in which the probability for ionization of the parent atoms by a single HCP was measured as a function of HCP amplitude. Previous work using higher-*n* atoms and longer-duration HCPs ($T_p \gtrsim 2$ ns) has shown that CTMC simulations are able to accurately predict absolute ionization and survival probabilities [4]. Thus by comparing theory and experiment, it is possible to determine the actual impulse delivered by a given HCP. If it is then assumed that the time dependence of the electric field mirrors that of the pulse applied to the HCP electrode, an estimate of the amplitude of the applied field can be obtained.

The number, and excited-state distribution, of Rydberg

atoms remaining in the experimental volume following application of the HCPs is measured, after a time delay of $\sim 6\mu$s, using selective field ionization (SFI). The time delay discriminates against free low-energy electrons produced by HCP-induced ionization which, tests showed, have a residence time of $\lesssim 5\mu$s in the interaction region. For SFI, a slowly varying (~ 0.5-μs rise time) positive voltage ramp is applied to the lower interaction-region electrode. Electrons resulting from field ionization are accelerated to, and detected by, a particle multiplier. Because atoms in different Rydberg states ionize at different applied fields, measurement of the field ionization signal as a function of time, i.e., of applied field, provides information on the excited-state distribution of those atoms present at the time of application of the SFI ramp. Measurements in which no HCPs are applied are interspersed at routine intervals during data acquisition to monitor the number of Rydberg atoms initially created by the laser. The Rydberg atom survival probability is determined by taking the ratio of the Rydberg atom signals observed with and without HCP application.

III. RESULTS AND DISCUSSION

Survival probabilities measured following application of trains of 20 and 50 equispaced, unidirectional HCPs are presented in Figs. 2(a) and 2(b) respectively, as a function of the pulse repetition frequency v_p (expressed in MHz and in scaled units) for several different HCP amplitudes. As might be expected, significantly larger HCP amplitudes are required to obtain a given fractional ionization when using 20 HCPs than when using 50 HCPs. The data show that the survival probability depends markedly on the pulse repetition frequency and a pronounced maximum is evident at scaled frequencies $v_0 \sim 1.3$. The survival probability at the maximum is surprisingly large. A HCP amplitude of 180 mV cm^{-1} corresponds to a scaled momentum transfer $\Delta p_0 \equiv \Delta p/p_n = n\Delta p \simeq 0.33$, suggesting that 50 HCPs should be more than sufficient to ionize essentially all the atoms present.

The survival probabilities observed after application of 20 and 50 HCPs that alternate in sign are shown in Figs. 3(a) and 3(b) respectively, as a function of pulse repetition frequency. (The pulse repetition frequency v_p is taken to be $1/T$ where, as shown in Fig. 1, T is the time between adjacent HCPs.) The survival probability again depends strongly on v_p but, in contrast to the data for unidirectional HCPs, no broad peak in the survival probability is evident. Rather, the survival probabilities generally increase with increasing pulse repetition frequency. A small local maximum in survival probability is observed, however, for scaled frequencies $v_0 \sim 1$.

Figures 2 and 3 include the results of 3D CTMC simulations that are described in more detail elsewhere [4]. Briefly, for unidirectional HCPs, these simulations make use of the Hamiltonian

$$H(t) = H_{\rm at} + zF(t) \simeq H_{\rm at} + z\sum_{j=1}^{N} F_{\rm HCP}(t - jv_T^{-1}), \qquad (1)$$

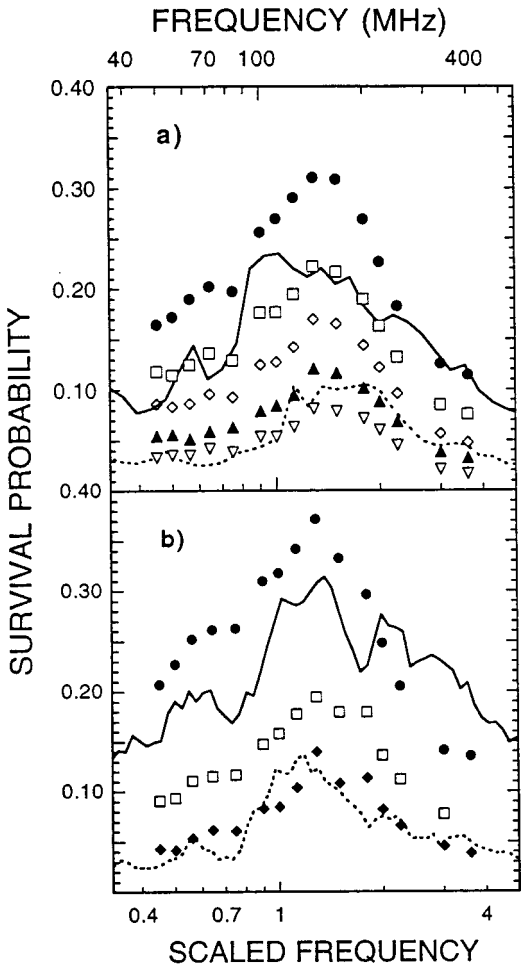

FIG. 2. (a) Rb($390p$) Rydberg atom survival probability following application of twenty unidirectional HCPs with peak fields of (●), 200; (□), 225; (◇), 250; (▲), 275; and (▽), 300 mV cm^{-1} as a function of pulse repetition frequency, expressed in MHz and scaled units $v_0 = v_p/v_n$. The figure includes the results of CTMC simulations [for Rb($390p$) atoms] that use the measured HCP profile and pulse amplitudes of (——) 200 and (– – –) 275 mV cm^{-1}, respectively. (b) Survival probability following application of 50 unidirectional HCPs with peak fields of (●), 120; (□), 150; and (◆), 180 mV cm^{-1}. The results of CTMC simulations for pulse amplitudes of (——) 120 and (– – –) 180 mV cm^{-1} are also shown.

where $F_{\rm HCP}$ is the field of a single pulse and N is the number of applied HCPs. The atomic Hamiltonian $H_{\rm at}$ is given in cylindrical coordinates (z,ρ,ϕ) by

$$H_{\rm at} = \frac{p_z^2 + p_\rho^2}{2} + \frac{L_z^2}{2\rho^2} + V_{\rm at}(\sqrt{z^2+\rho^2}), \qquad (2)$$

where L_z is the z component of the angular momentum, which is a constant of motion, and, for the present work, has only very small scaled values $L_{z0} \lesssim 5 \times 10^{-3}$. For $V_{\rm at}$ a one-electron pseudopotential is used that yields accurate quantum defects and that satisfies the correct boundary conditions at large and small radii. The profile $F_{\rm HCP}$ is assumed to mirror that of the pulse applied to a HCP electrode. For alternating HCPs, the Hamiltonian

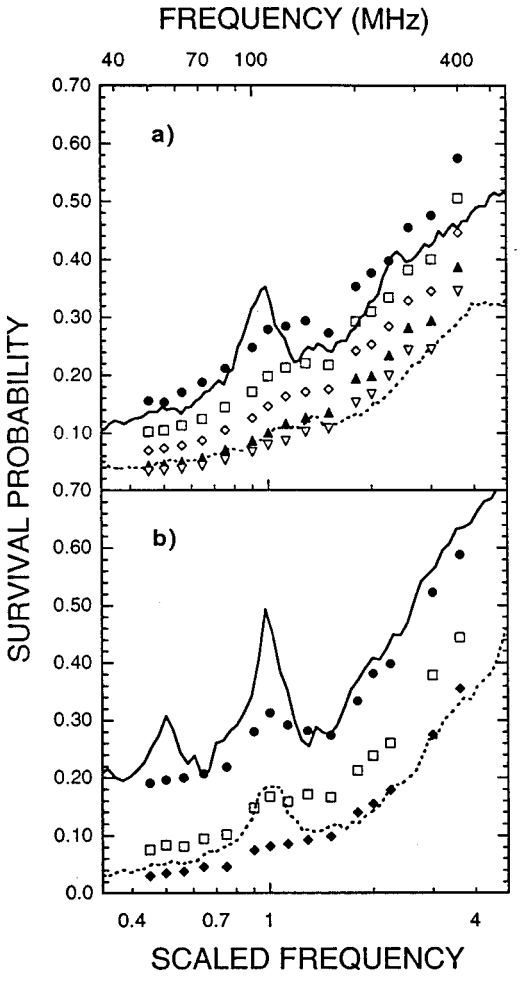

FIG. 3. (a) Rb($390p$) Rydberg atom survival probability following application of 20 alternating HCPs with peak fields of (●), 200; (□), 225; (◇), 250; (▲), 275; and (▽), 300 mV cm^{-1} as a function of pulse repetition frequency. The solid line shows the results of CTMC simulations that use the measured HCP profile and pulse amplitudes of (——) 200 and (– – –) 275 mV cm^{-1}. (b) Survival probability following application of 50 alternating HCPs with peak fields of (●), 120; (□), 150; and (◆), 180 mV cm^{-1}. The results of CTMC simulations for pulse amplitudes of (——) 120 and (– – –) 180 mV cm^{-1} are also shown. The CTMC calculations assume the presence of a residual stray field sufficient to ionize atoms with $n \gtrsim 1200$.

$$H(t) \simeq H_{\rm at} + z \sum_{j=1}^{N} (-1)^{j+1} F_{\rm HCP}(t - j v_T^{-1}) \qquad (3)$$

is used, where N is even. The calculations assume an isotropic phase-space microcanonical ensemble with classical angular momenta $1 \leqslant L \leqslant 2$ corresponding to the initial laser-excited $\ell = 1$ quantum state with a statistical population of m substates.

The CTMC simulations provide good agreement with the data without recourse to any adjustable parameters. In the case of alternating HCPs, however, the calculated survival probability was found to be quite sensitive to the presence of small residual fields. No similar sensitivity exists for unidirectional HCPs since the time-averaged electric field associated with the train of pulses $F_{\rm av} = v_p \Delta p$ is much larger than any residual field. In turn, the time-averaged field for alternating pulses is $F_{\rm av} = 0$ and, therefore, stray fields play a comparatively larger role. The CTMC results in Fig. 3 assume the presence of a small residual field sufficient to ionize atoms with $n \gtrsim 1200$. The size of the calculated peak predicted at scaled frequencies $v_0 \sim 1$ is somewhat larger than that measured. In addition, the calculations exhibit a local maximum at $v_0 \sim 0.5$ that is not visible in the measurements. Given the sensitivity to stray fields, these differences could be the result of small field inhomogeneities in the experimental volume.

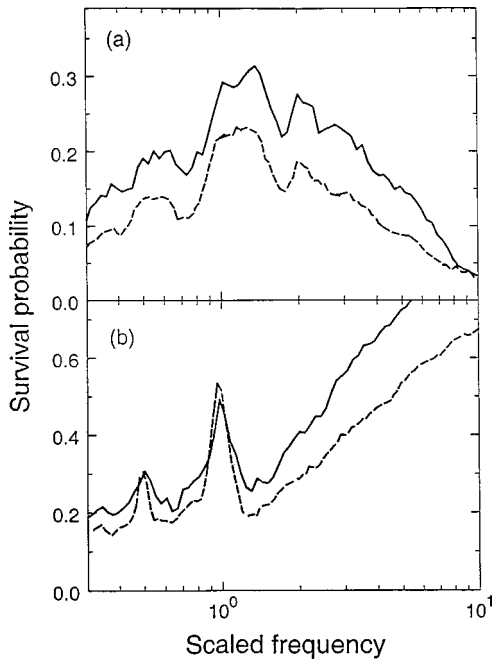

FIG. 4. Calculated Rydberg atom survival probabilities following application of 50 (a) unidirectional and (b) alternating HCPs of amplitude 120 mV cm^{-1} as a function of the scaled pulse repetition frequency. The solid lines show the results of CTMC simulations for Rb($390p$) atoms that use the measured HCP profile. Results for H($390p$) atoms obtained using the δ-function impulse model are indicated by the dashed lines.

The origin of the features present in the data was examined by considering the behavior of the system when it is subject to a large number of HCPs. To investigate this high-N limit, the simplified model of a hydrogen atom ($V_{\rm at} = -1/\sqrt{\rho^2 + z^2}$) subject to δ-function impulses was employed [i.e., replacing $F_{\rm HCP}(t)$ by $\Delta p\, \delta(t)$ in Eqs. (1) and (3)]. As illustrated in Fig. 4, survival probabilities calculated for H($390p$) using this model and for Rb($390p$) using finite-width pulses display the same general structure demonstrating that use of the simplified model is reasonable. The predicted survival probabilities, however, lie a little below those obtained for finite-width pulses because the finite-width cuts off the higher frequencies in the perturbation.

The broad maximum in the survival probability for unidirectional pulses comprises a series of overlapping peaks whose origin can be traced by analyzing Poincaré surfaces of section. We have shown that sizable stable islands enclosed

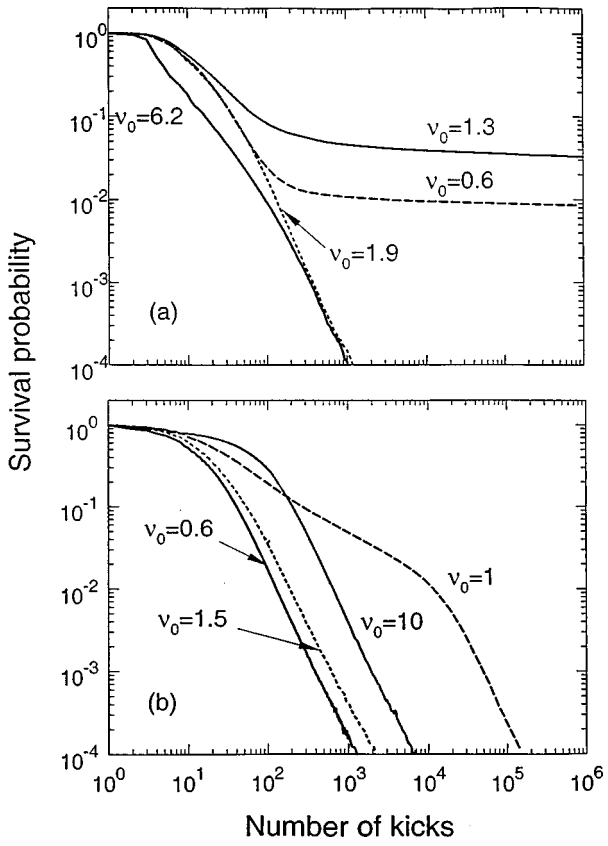

FIG. 5. Calculated survival probabilities for a 3D H($390p$) atom subject to a train of (a) unidirectional and (b) alternating δ-function kicks with various scaled frequencies v_0 as a function of the number N of kicks.

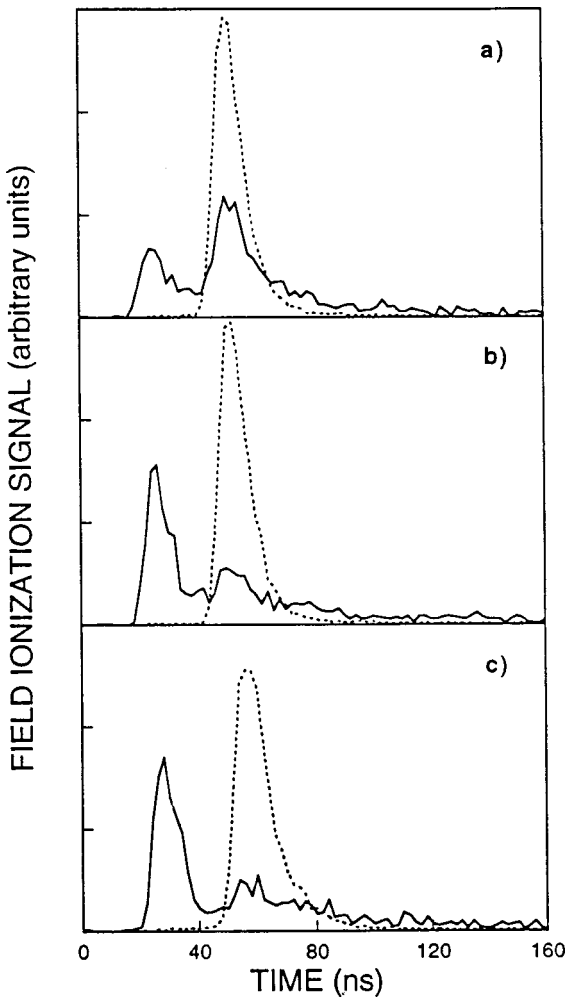

FIG. 6. SFI profiles observed for surviving atoms following application of 50 unidirectional HCPs with scaled pulse repetition frequencies v_0 of (a) 1.3 and (b) 0.5, respectively; and (c) following application of 50 alternating HCPs with $v_0=1$. In each case the HCP amplitudes are sufficient to ionize ~90% of the parent atoms. The dashed line in each data set corresponds to the SFI profile observed for the parent Rb($390p$) atoms. To better compare the shapes of the various profiles, the SFI spectra are normalized to equal areas.

by Kolmogorov-Arnold-Moser (KAM) tori exist that are associated with dynamical stabilization [4]. For certain values of frequency, the initial state of the electron overlaps stable islands in phase space and stabilization is obtained by trapping the phase-space trajectories within these islands. This is illustrated in Fig. 5(a), which shows the calculated survival probability as a function of the number N of kicks for several values of scaled frequency v_0. When the initial state lies within a stable island, the survival probability, after initially decreasing, becomes steady, even for $\gtrsim 10^6$ kicks, providing clear evidence of dynamical stabilization. For other values of frequency the initial state lies in the chaotic sea. In this case, the survival probability decreases monotonically with increasing N, a characteristic of chaotic ionization.

Additional experimental evidence for dynamical stabilization and chaotic ionization is contained in the distribution of excited states following application of the HCP train. If dynamical stabilization occurs, the distribution of excitation energies of the surviving bound states should be sharply peaked near the initial energy. This behavior is confirmed by the SFI spectra shown in Fig. 6. In the absence of HCPs, the SFI spectrum comprises a single relatively narrow peak that corresponds to ionization of parent $390p$ atoms. The SFI profile observed following application of 50 HCPs with a scaled repetition frequency $v_0 \sim 1.3$ (for which the survival probability is near maximum) and an amplitude sufficient to ionize ~90% of the parent atoms is broader than that for the parent atoms. This indicates that the HCP application populates a range of final n states. The majority of the atoms, however, ionize at field strengths comparable to those of the parent atoms, demonstrating that the n distribution of the surviving atoms is peaked at a value of n similar to that of the parent atoms, as is expected if dynamical stabilization is occurring. (The sharp peak in the SFI profile at early times, i.e., at small values of applied field, is an artifact of the SFI process and results because the threshold field for ionization scales as n^{-4}. The ionization of the highest n atoms is therefore compressed into a narrow range of applied fields, i.e., a narrow time range.) The SFI profile for a scaled repetition frequency $v_0 \sim 0.5$ (where dynamical stabilization is not expected), contains no pronounced feature at field strengths near those characteristic of parent-state ionization. Rather,

the SFI spectrum is dominated by the ionization of very-high-n atoms, which is consistent with chaotic migration from the initial state to highly excited levels near the ionization threshold.

The use of alternating kicks leads to a marked change in the pulse repetition frequency dependence of the Rydberg atom survival probability, which shows a general increase with increasing scaled frequency. Such behavior is expected. At high scaled frequencies, the time delay between adjacent kicks becomes very short and the effect of one kick is, in essence, immediately reversed by the next (equal but opposite) kick. (Indeed, tests in which the atoms were subject to 50 pairs of very closely spaced equal but opposite kicks showed that the survival probability was large, $\gtrsim 0.8$, and essentially independent of the pulse pair repetition frequency.) The data do, however, provide evidence for a local maximum in survival probability for scaled frequencies $v_0 \sim 1$, and this is well reproduced by the CTMC simulations. This feature is suggestive of dynamical stabilization. To explore this possibility further, the N dependence of the survival probability was explored using the δ-function impulse model. These calculations [Fig. 5(b)] indicate that, in contrast to the case for unidirectional kicks, the survival probability simply decreases monotonically with increasing N for all scaled frequencies, even those in the vicinity of $v_0 \sim 1$. (The rate of decrease, however, is significantly lower in this regime leading to the local maximum in the observed survival probability.) Figure 5(b) suggests either that dynamical stabilization does not occur or that it occurs with a very small probability. This result is, at first sight, surprising since the survival probabilities after 50 unidirectional and alternating pulses depicted in Figs. 2 and 3 have the same order of magnitude. This can be attributed to the fact that the effect of a kick is partially reversed by the next kick for alternating pulses and that the chaotic diffusion rate is smaller than that for unidirectional pulses. Only after a very large number of kicks (much larger than 50 kicks) does the effect of dynamical stabilization become evident and the survival probability for unidirectional pulses surpass that for alternating pulses.

In an attempt to gain insight into the physical origin of the local maximum at $v_0 \sim 1$ for alternating pulses, Poincaré surfaces of section were examined for a wide range of cuts in ρ and p_ρ. Since L_z is a constant of motion, the 3D kicked atom represents a time-dependent dynamical system with two degrees of freedom (a four-dimensional phase space), which can be mapped into a time-independent 2 and 1/2 degree of freedom system (the time being the additional ''1/2'' degree of freedom). The single-period (two kicks) evolution associated with the simplified Hamiltonian is given by a map of phase-space coordinates

$$M = M_{\mathrm{Coul}} M_{+\Delta p} M_{\mathrm{Coul}} M_{-\Delta p}, \tag{4}$$

where M_{Coul} describes the evolution of the Coulomb orbit between HCPs and $M_{\pm\Delta p}$ describes the effect of the impulse. M maps the four-dimensional phase space (ρ, z, p_ρ, p_z) onto itself. The evolution of the phase-space coordinates after N kicks is simply given by $M^{N/2}$, allowing the stability of the system in the limit $N \to \infty$ (typically $N \gtrsim 10^6$) to be examined in detail.

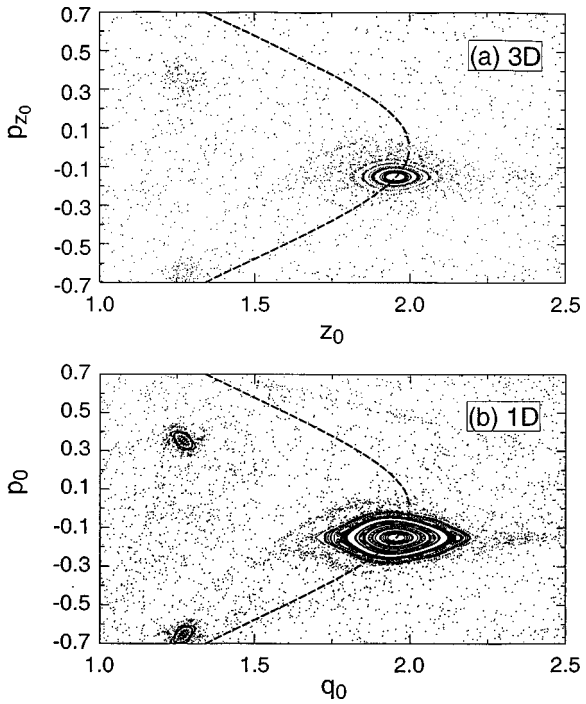

FIG. 7. Poincaré surface of section for (a) the 3D and (b) the 1D hydrogen atom subject to a series of alternating δ-function kicks with $\Delta p_0 = 0.3$. The 3D slice is taken at $\rho_0 = 0.1$ and $p_{\rho 0} = 0$. The time cuts are taken immediately before the first, third, fifth... kicks. The dashed line in the figure corresponds to the initial state of the electron.

The stroboscopic snapshots taken after each application of M lie on a four-dimensional (4D) manifold. Visualization in terms of Poincaré surfaces of section requires the reduction to a two-dimensional manifold by slicing the 4D manifold into layers defined by fixed coordinates $(\rho \pm \Delta\rho, p_\rho \pm \Delta p_\rho)$. Figure 7(a) displays one such slice of the 3D kicked atom for the scaled values $\rho_0 = 0.1$ and $p_{\rho 0} \equiv n p_\rho = 0.1$. Surprisingly, sizable closed loops that resemble cuts of KAM tori are evident. However, the analysis of dynamical stabilization in this high-dimensional system turns out to be complicated.

For a comparative analysis of the phase-space structure of the 3D kicked atom, CTMC simulations were undertaken for a simpler 1D ''atom'' [5,6] subject to a periodic sequence of alternating δ-function kicks whose dynamics is governed by the Hamiltonian

$$H(t) = \frac{p^2}{2} - \frac{1}{q} + \frac{\Lambda^2}{2q^2} - q\Delta p \sum_{j=1}^{N} (-1)^{j+1} \delta(t - j v_T^{-1}), \tag{5}$$

where q and p denote the position and momentum of the electron, respectively, and $\Lambda \to 0$ is a quasi-angular momentum. Figure 7(b) shows that the Poincaré map for the 1D kicked atom is very similar to that for the 3D atom shown in Fig. 7(a). This is, perhaps, not surprising given that the Poincaré surface of section for the 3D system was obtained by taking a cut at small $\rho_0 (\sim 0.1)$ and $p_{\rho 0} (\sim 0)$ close to the phase space of the one-dimensional atom. In each case, the center of the main ''island'' corresponds to a periodic orbit. This periodic orbit can be identified with the help of its pro-

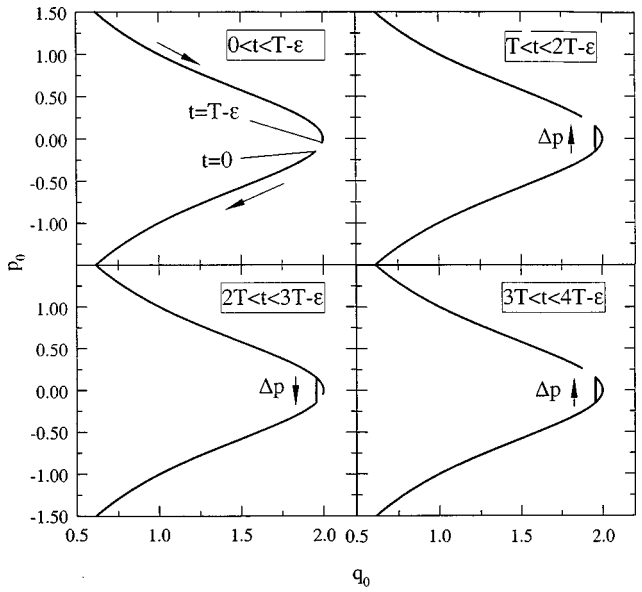

FIG. 8. Projection of dominant 1D periodic ''orbit'' onto the p, q plane for alternating δ-function kicks with $\Delta p_0=0.3$ and $v_0=1$. Each successive orbit is shown separately to better visualize the behavior. The solid arrows indicate the direction of motion along the orbit.

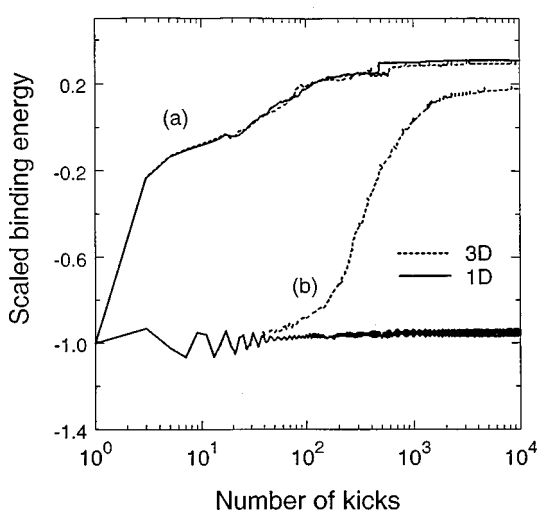

FIG. 9. Average binding energy just before the Nth kick as a function of the number of kicks for two ensembles of particles (see text) in the same initial energy level depicted in Fig. 7. The ensembles (a) within the chaotic sea and (b) near the periodic orbit correspond to initial conditions near $q_0=z_0=1.85$, $p_0=p_{z0}=+\sqrt{-1+(2/q_0)}$, and $p_0=p_{z0}=-\sqrt{-1+(2/q_0)}$, respectively.

jection onto the (q,p) plane [or (z,p_z) plane], which is shown in Fig. 8. To better visualize the behavior, different segments of the orbit are shown separately. Obviously, the electronic motion is confined to a single Coulomb ''orbit.'' This requires that the energy transferred to the excited electron by each impulse, $\Delta E=\Delta p^2/2+p(\pm\Delta p)$, be zero, i.e., that the electron momentum prior to the kick be $p=-(\pm\Delta p)/2$. The electron first completes the orbit in one direction, then in the other, the reversals being triggered by the alternating applied kicks $+\Delta p,-\Delta p,+\Delta p\ldots$ The reversals occur at the same coordinate q and simply change the direction of motion of the electron without changing its energy, i.e., its momentum changes from $-(\pm\Delta p)/2$ to $\pm\Delta p/2$. As expected, the dominant islands present in Fig. 7(b) where the cut is immediately before each positive kick ($\Delta p_0=+0.3$), are centered at a scaled initial momentum $p_0=-0.15$. Periodic orbits for $v_0=1$ for the 3D system can be identified for any slice in $(\rho\pm\Delta\rho,p_\rho\pm\Delta p_\rho)$. Other periodic orbits are evident in Fig. 7(b) as well.

The fundamental difference between the 1D and 3D phase-space structures is the stability properties of the islands. The 1D system features KAM tori, which are structurally stable and are confining. This means that any torus provides a globally impenetrable barrier against diffusion and that chaotic and regular regions remain well separated. In the 3D case, however, all chaotic regions are interconnected with each other, one manifestation of which is Arnold diffusion [7]. In the present case of alternating pulses, the islands that resemble tori are, in fact, ''leaky'' tori or cantori [7]. Simulations show that, indeed, the trajectories forming the closed loops in Fig. 7(a) only intersect the slice of the figure for a finite period of time after which they drift away and eventually become ionized. The slow drift motion of apparent KAM-like structures for alternating kicks has been observed before [8].

Leaky tori will slow down diffusion but cannot completely suppress it. Starting on a leaky torus, the energy diffusion will initially be slow. As the trajectory wanders toward the edge of the torus, it will eventually reach the interconnected global chaotic sea. This is accompanied by a transition from slow to fast diffusion. The latter is, to some extent, ''universal,'' i.e., independent of when and where the chaotic sea is being reached. This is illustrated in Fig. 9, where the energy diffusion of two large ensembles of initial conditions is followed as a function of time. Both ensembles of initial conditions lie on the same initial manifold (i.e., the dashed line in Fig. 7) and, initially, the scaled binding energy is $E_0=-1$. If the ensemble of initial conditions lies in the chaotic sea, a rapid energy diffusion of the system is observed until the continuum is reached. Only after the electrons have reached the continuum and are far from the Coulomb center does energy diffusion cease because alternating pulses cannot change the energy of a free electron. Remarkably, the 1D and 3D simulations are almost indistinguishable from each other, attesting to the ''universality'' of the fast chaotic motion. An entirely different picture emerges when the ensemble of initial conditions is placed in the region of the island associated with the leaky torus in the 3D case and the true KAM torus in the 1D case. In one dimension, KAM tori completely suppress diffusion and only fluctuation in energy around the initial value due to the quasiperiodic motion is observed. In the 3D case, the ensemble initially undergoes quasiperiodic motion before slow diffusion away from the leaky tori sets in after about 100 kicks.

The local narrow maximum in the experimental and theoretical survival probability evident in Fig. 3 at $v_0=1$ after 50 kicks should therefore be viewed as a signature of the

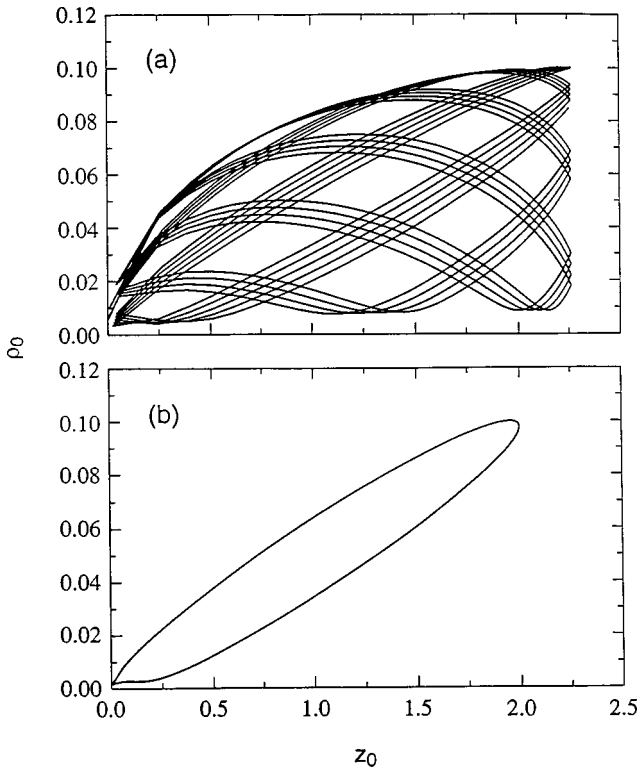

FIG. 10. Projection of the dominant periodic orbit on the (z,ρ) plane for (a) unidirectional and (b) alternating pulses with strength $\Delta p_0=0.3$ and initial conditions such that $\rho_0=0.1$ and $p_{\rho 0}=0$. The periodic orbit is followed for many pulses in the train.

delayed onset of chaotic diffusion due to the motion on leaky tori, rather than as a signature of true stabilization. However, for the time interval prior to the onset of chaotic diffusion accessible in the current experiment, the survival probabilities for the atom driven by unidirectional and alternating kicks can be comparable in magnitude. This is precisely what is observed in Fig. 3. The presence of slow diffusion and absence of stabilization for alternating pulses is experimentally confirmed by the SFI profiles measured following application of 50 (alternating) HCPs (see Fig. 6), which contain no pronounced feature at field strengths near those characteristic of parent-state ionization. Instead, the SFI spectrum is dominated by ionization of very-high-n atoms, pointing to diffusive motion toward higher-n levels.

The stabilization observed for unidirectional pulses in 3D and the lack thereof for alternating pulses poses a puzzling question: precisely what mechanism is responsible for this quite different behavior? A partial answer to this question is provided by comparing the excursions along the ρ direction (see Fig. 10) of the dominant periodic orbits for these two cases. For alternating pulses, the periodic orbit is completely degenerate: it is composed of a single Coulomb orbit that has the same frequency $v=v_p=v_n$ in all degrees of freedom. In contrast, the periodic orbit for unidirectional pulses clearly involves two frequencies: the frequency of the pulses v_p, which is larger than the Coulomb frequency v_n, and a slower frequency that corresponds to precession of the Coulomb orbit. A frequency analysis of the orbit indicates that the latter is equal to the Stark precession frequency v_{Stark} associated with the averaged electric field of the train of pulses $F_{\mathrm{av}}=v_p\Delta p$ [in first-order perturbation theory, $v_{\mathrm{Stark}}=3F_{\mathrm{av}}n/(2\pi)$]. This additional electric field, which is absent for alternating pulses, clearly plays a crucial role in the stabilization of the atom for unidirectional pulses. It provides for the existence of a set of incommensurate frequencies of the system, which is essential for the existence of KAM tori. On the other hand, the absence of an average electric field for alternating kicks leads to degeneracy and to leaky remnants of tori. This observation suggests that the dynamical properties of the kicked atom for alternating kicks could be changed substantially by adding an additional dc field, which could be explored in future studies. Furthermore, experimental studies of the kicked atom have so far utilized initial states with a nearly zero centrifugal barrier in Eq. (2): i.e., the atom is initially on an np state for which $L_{z0}\sim 0$. Theoretical studies of the kicked atom for large values of L_{z0} indicate that the centrifugal barrier can stabilize the atom for alternating pulses [6].

The present work reaffirms that high-n Rydberg atoms subject to a train of HCPs provide an excellent model system for studying the behavior of periodically driven systems. Measurements with alternating kicks provide an opportunity to model the behavior of atoms subject to intense electromagnetic radiation and promise new insights into intense field stabilization [9,10]. CTMC simulations that employ realistic potentials and pulse shapes provide results that are in good agreement with the experimental data indicating that, for the present range of field strengths, interaction times, and pulse repetition frequencies, classical-quantum correspondence holds and quantum effects are negligible. However, theory predicts that at higher scaled frequencies, $v_0\gtrsim 15$, classical-quantum correspondence might break down as a result of quantum localization [5] when a large number of unidirectional kicks is applied. Further insights into dynamical stabilization might also be obtained by studies involving high-m atoms, which can be created by application of a pulsed ''dc'' field [8]. Theoretical studies indicate that the survival probabilities for such states are significantly higher than for low-m states. Because the harmonic content of the driving field can be varied by changing the shape and/or width of the HCPs, such measurements might also illuminate the more general problem of atomic excitation by multifrequency ''colored'' fields. It will also be interesting to examine how the system behaves in making the transition between the two HCP trains studied here, i.e., as the amplitude of every other HCP in the train is first reduced to zero and then increased in the opposite sense.

ACKNOWLEDGMENTS

The experimental work was supported by the National Science Foundation and the Robert A. Welch Foundation. The theoretical work was funded by the Division of Chemical Sciences, Office of Basic Energy Sciences, USDOE, under Contract No. DE-AC05-96OR-22464, managed by Lockheed Martin Energy Research Corporation, the NSF, and the FWF.

[1] P. M. Koch and K. A. H. van Leeuwen, Phys. Rep. **255**, 289 (1995); R. V. Jensen, Nature (London) **355**, 311 (1992).

[2] F. Moore, J. Robinson, C. Bharucha, P. Williams, and M. Raizen, Phys. Rev. Lett. **73**, 2974 (1994); B. G. Klappauf, W. H. Oskay, D. A. Steck, and M. G. Raizen, *ibid.* **81**, 4044 (1998).

[3] S. A. Gardiner, J. I. Cirac, and P. Zoller, Phys. Rev. Lett. **79**, 4790 (1997).

[4] M. T. Frey, F. B. Dunning, C. O. Reinhold, S. Yoshida, and J. Burgdörfer, Phys. Rev. A **59**, 1434 (1999); S. Yoshida, C. O. Reinhold, P. Kristöfel, J. Burgdörfer, S. Watanabe, and F. B. Dunning, *ibid.* **59**, R4121 (1999); C. O. Reinhold, J. Burgdörfer, M. T. Frey, and F. B. Dunning, Phys. Rev. Lett. **79**, 5226 (1997); M. T. Frey, F. B. Dunning, C. O. Reinhold, and J. Burgdörfer, Phys. Rev. A **53**, R2929 (1996).

[5] S. Yoshida, C. O. Reinhold, and J. Burgdörfer, Phys. Rev. Lett. **84**, 2602 (2000).

[6] G. Casati, I. Guaneri, and G. Mantica, Phys. Rev. A **50**, 5018 (1994).

[7] See, e.g., A. Lichtenberg and M. Liebermann, in *Regular and Stochastic Motion* (Springer, New York, 1992).

[8] J. Burgdörfer, Nucl. Instrum. Methods Phys. Res. B **42**, 500 (1989).

[9] H. Wiedemann, J. Mostowski, and F. Haake, Phys. Rev. A **49**, 1171 (1994).

[10] B. E. Tannian, C. L. Stokely, F. B. Dunning, C. O. Reinhold, and J. Burgdörfer, J. Phys. B **32**, L517 (1999).